Defence Technology xxx (xxxx) xxx

Contents lists available at ScienceDirect

Defence Technology

journal homepage: www.elsevier.com/locate/dt

Formation and impact-induced separation of tandem EFPs

Hong-bing Ma, Yuan-feng Zheng*, Hai-fu Wang, Chao Ge, Cheng-hai Su

State Key Laboratory of Explosion Science and Technology, Beijing Institute of Technology, Beijing 100081, China

ARTICLE INFO

Article history:
Received 9 July 2019
Received in revised form
24 August 2019
Accepted 5 September 2019
Available online xxx

Keywords:
Shaped charge
Liner
Tandem EFPs
Formation
Separation

ABSTRACT

The formation and separation behaviors of tandem EFPs are studied by the combination of experiments and simulations. The results show that different formation and separation processes can be obtained by adjusting the double-layer liners, and simulations agree with experiments well. Then, the interaction process between the two liners is discussed in details, and the formation and separation mechanism are revealed. It can be found that there are four phases in the formation and separation processes, including impact phase, propulsion phase, slide phase and free flight phase. During the impact phase, the velocities of two liners rise in turns with kinetic energy exchange. In the propulsion phase, the axial impact becomes insignificant, but the radial interaction between two liners influences the appearance of tandem EFPs. Meanwhile, it should be mentioned that the inner surface of foregoing EFP remains to be in contact with the outer surface of following EFP in the propulsion phase, and the following one would continue to push the foregoing one for about 10μ to 20 μs, causing the velocities of following and foregoing EFPs gradually decreasing and increasing respectively. In the slide phase, an obvious relative movement occurs between the two EFPs, and there would be barely kinetic energy exchange. Then, the two EFPs separate gradually and get into the phase of free flight. Generally, if the outer and inner liners have the same thickness, the outer copper-inner copper liners form two long EFPs, the outer copper-inner steel liners become a foregoing short steel EFP and a following long copper EFP, and the outer steel-inner copper liners produce a foregoing long copper EFP and a following conical steel EFP. In addition, thickness match also has an important impact on formation appearance and separation process for both outer copper-inner copper liners and outer steel-inner copper liners. With the thickness ratio of outer liner to inner liner decreasing, the length and length-diameter ratio of both foregoing and following EFPs increase gradually.

1. Introduction

Explosively Formed Projectile (EFP) has been used widely in military to attack medium and light armored targets, due to its high speed, high mass conversion and satisfied flight stability. However, the small length-diameter ratio and limited penetration capability of a single EFP greatly restrict the development and improvement of the shaped charge warhead technology. In order to solve this problem, one promising way is to study the collinear multi-EFPs warhead technology. This technology would obtain collinear multi-EFPs just by replacing the single liner with layered multi-liners, without changing the general structure of the shaped charge. The multi-EFPs utilize the advantage of the single EFP for its high speed and fine flight stability, and also overcome the problem of small length-diameter ratio.

Because of the benefits discussed above, the multi-EFPs have been studied intensively in recent years. Tosello. R et al. have studied the underwater movement behavior of tandem EFPs formed by tantalum-nickel double-layer liners. The results show that the foregoing EFP creates a channel in water, thus significantly reducing the move resistance for the following EFP [1]. Weimann. K et al. design tantalum-iron double-layer liners, which would deform under shaped charge effect and become a large length-diameter ratio penetrator with tantalum body and iron rear [2]. Fong. R et al. have studied the aerodynamic stabilization of multi-EFPs in order to obtain a deeper penetration depth at a small stand-off and improve the multiple impact capability at a large stand-off [3]. Zheng Yu et al. have researched the influence of

* Corresponding author.
E-mail address: zhengyf@bit.edu.cn (Y.-f. Zheng).
Peer review under responsibility of China Ordnance Society

https://doi.org/10.1016/j.dt.2019.09.003

materials on the formation behavior of tandem EFPs, and the result shows that double liners can be separated into two projectiles with certain configuration and liner materials. The combination of liner material and the ignition position have great influences on the formation of tandem EFP [4]. Li Huiming et al. have carried out research on the influence of materials on the penetration characteristics of tandem EFPs, the corresponding result indicates that the penetration can be improved by using materials with low density, good extensibility and low strength for outer layer and low density, good extensibility for inner layer [5]. Long Yuan et al. have discussed the influence of curvature radius on the formation and penetration characteristics of tandem EFPs, and the conclusion shows that the penetrator has a good shape and the maximum penetration depth is about 1 time charge caliber when the relative value of liner curvature radius is located in 0.67–0.93 [6,7]. Wang Zhe et al. have established the velocity analysis model of tandem EFPs, and the influence characteristics on velocity are revealed [8]. He Jing et al. have simulated the formation of shaped charge with double liners, and the result shows that the double liners can form separated EFPs with good appearance. However, the addition of material between two liners would lead to separated EFPs with poor formation [9].

It can be seen that the research in this field mainly focuses on the effects of liner materials, curvature radius, and other factors on the formation and penetration phenomena of tandem EFPs. However, the formation and separation mechanisms of collinear tandem EFPs have not been studied profoundly. As such, the formation behavior of tandem EFPs is studied and verified experimentally and numerically in this paper. Then, the formation and separation mechanisms are stressed, and the influencing mechanisms of material and thickness match on the formation and separation are analyzed.

2. Formation and separation behaviors

2.1. Experimental setup

The warhead, depicted in Fig. 1, mainly consists of an explosive, double-layer liners and baffle ring. The high explosive 8701 is poured into the press mold and a pressure load of 200 MPa is applied at room temperature, thus the high explosive charge has a length of 50 mm, a diameter of 50 mm, a mass of 158 g, and a density of 1.71 g/cm^3. The explosive would be centrally initiated through a simple detonator at the bottom. In the experiments, four types of double-layer spherical segment liners are used, including outer copper-inner copper (type A), outer copper-inner 45# steel (type B), outer 45# steel-inner copper (type C), and outer copper-inner aluminum (type D). It should be appointed that the liner closing to the explosive is considered as the outer liner and the other one is marked as the inner liner. All the liners have a curvature radius of 45 mm. The annular baffle ring, made of 45# steel and used to prompt the detonation products flowing radially, is 2.5 mm thick and 3.43 mm high. The typical photographs of warheads are shown in Fig. 2. The schematic diagram of the experimental setup is shown in Fig. 3(a), and the corresponding photograph is shown in Fig. 3(b). As can be seen, the warhead is positioned on a long and hollow cylinder, and an X-ray system is used to capture the formation of tandem EFPs at times of t_1 and t_2, where the time $t_0 = 0$ corresponds to the moment of the detonator being initiated. The protective plate is also used to prevent the tandem EFPs from impacting the cement floor. The detailed experimental conditions are listed in Table 1.

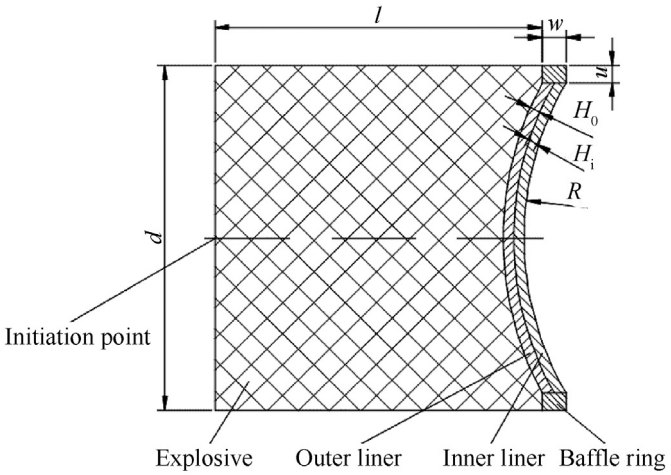

Fig. 1. Sketch of warhead: parameters of d, l, u, w, H_o, H_i, and R are explosive diameter, explosive length, baffle ring thickness, baffle ring height, outer liner thickness, inner liner thickness, and curvature radius, respectively.

2.2. Simulation method

Four types of warheads are modelled in AUTODYN-3D, corresponding to four conditions listed in Table 1 respectively. The Lagrange algorithm is employed, and the model is designed quarterly because of the symmetry. Take type B for example, the mesh numbers of explosive, outer liner, inner liner, and baffle ring are 35190,3703,3703 and 1288 respectively. A typical model is given in Fig. 4.

The JWL equation of state is used to describe the expansion of detonation products for high energy explosive material 8701, according to the following form:

$$P = A\left(1 - \frac{\omega}{R_1 V}\right)e^{-R_1 V} + B\left(1 - \frac{\omega}{R_2 V}\right)e^{-R_2 V} + \frac{\omega E_0}{V} \tag{1}$$

where A, B, R_1, R_2 and ω are material constants, E_0 represents the detonation energy per unit volume and V is the relative volume. The corresponding parameters of 8701 explosive are from Ref. [10], in which $\rho_0 = 1.71$ g/cm^3, $A = 524.23$ GPa, $B = 7.678$ GPa, $R_1 = 4.2$, $R_2 = 1.1$, $\omega = 0.34$, $E_0 = 8.499$ GPa, CJ detonation pressure $P_{CJ} = 28.6$ GPa, and detonation velocity $D = 8315$ m/s.

The SHOCK equation of state is used to describe the behavior of materials, including copper and 45# steel. While, the Tillotson equation of state is adopted to provide an accurate description of aluminum, which would expand and change of phase in cases where the shock energy has been sufficient to melt or vaporize the material.

The Johnson-Cook material model is used to represent the strength behavior of materials, typically metals, subjected to large strains, high strain rates and high temperatures. Such behavior might arise in problems of intense impulsive loading due to high velocity impact. With this model, the yield stress varies depending on strain, strain rate and temperature. The model defines the yield stress σ as:

$$\sigma = [A' + B'\varepsilon_p^n][1 + C\ln\frac{\dot{\varepsilon}_p}{\dot{\varepsilon}_0}][1 - (\frac{T - T_{room}}{T_{melt} - T_{room}})^m] \tag{2}$$

where A', B', C, n and m are material constants. ε_P is the effective plastic strain. $\dot{\varepsilon}_0 = 1\text{s}^{-1}$ is the reference plastic strain rate. T_{melt} and T_{room} denote the melting and room temperatures, respectively.

The detailed parameters for copper and 45# steel are listed in Table 2 [11,12]. While, the parameters for aluminum are listed in

Please cite this article as: Ma H-b et al., Formation and impact-induced separation of tandem EFPs, Defence Technology, https://doi.org/10.1016/j.dt.2019.09.003

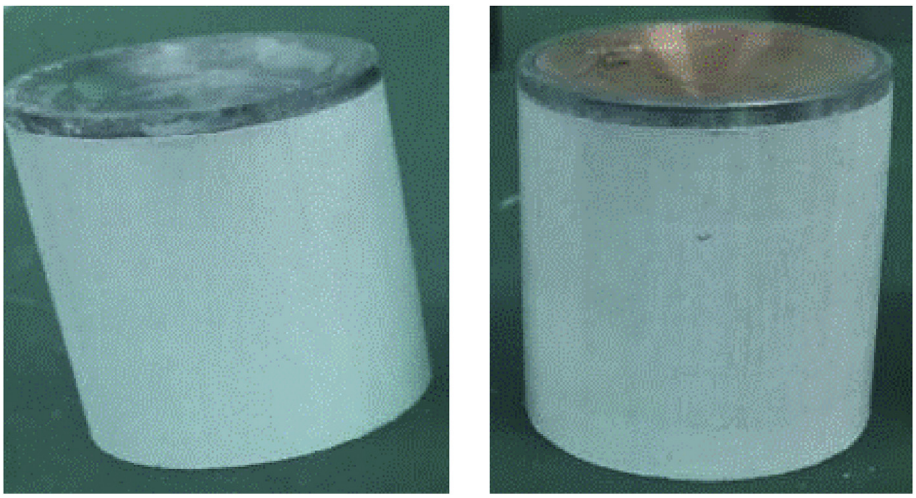

Fig. 2. Photographs of typical warheads for tandem EFPs formation.

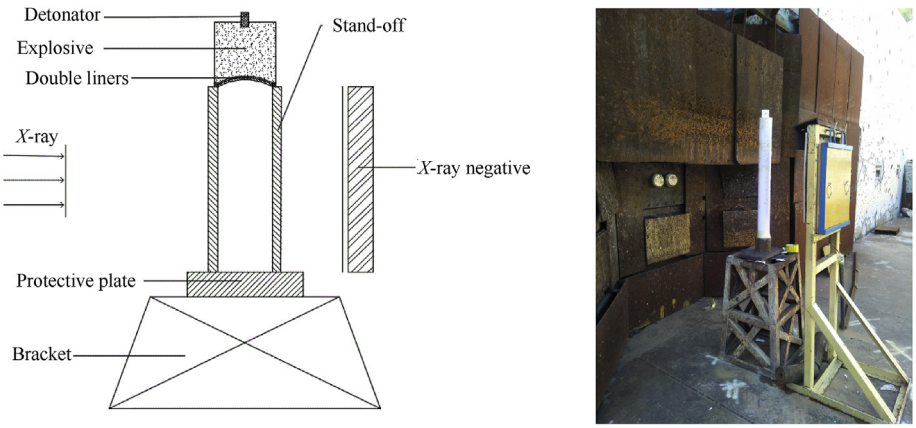

(a) Principle (b) Setup.

Fig. 3. Experimental principle and setup of X-ray: (a) principle; (b) setup.

Table 1
Experimental conditions of tandem EFPs formation.

No.	Type	Measured parameters					
		Outer liner			Inner liner		
		Material	Thickness/mm	Mass/g	Material	Thickness/mm	Mass/g
1	A	Copper	2.0	30.3	Copper	1.0	15.1
2	B	Copper	1.5	22.8	45#Steel	1.5	20.0
3	C	45#Steel	1.5	20.0	Copper	1.5	22.8
4	D	Copper	1.5	22.8	Aluminum	1.5	7.08

Table 3, where a, b, A', B', α, β are empirical constants, e_s is the minimum gasification energy of local gasification, e_{sd} is the gasification energy of complete gasification, and e_v is the gasification energy of material at zero pressure [13].

2.3. Comparison between experimental and simulated results

A comparison between the experimental and simulated results is presented in Table 4. The resolution of the experimental image is 251 × 251 DPI, and the exposure times of X-ray are 150 μs and 210 μs, respectively. In the X-ray photographs of type A liners, it is observed that the inner copper liner forms a foregoing EFP with a low length-diameter ratio, whereas the outer liner becomes a following EFP with a high length-diameter ratio.

As for the type B liners, it is evident that the EFP formed by the inner steel liner has a low length-diameter ratio, while the EFP formed by the outer copper liner has a high length-diameter ratio. Furthermore, the foregoing EFP formed by the inner steel liner has a hollow structure, which wraps around the following EFP formed by copper during the formation and flight. The two EFPs then begin to move as a united entity, whose structure is slightly elongated over time.

In regards to type C liners, the result shows that the inner copper liner forms a long and slender penetrator in front, while the outer

Please cite this article as: Ma H-b et al., Formation and impact-induced separation of tandem EFPs, Defence Technology, https://doi.org/10.1016/j.dt.2019.09.003

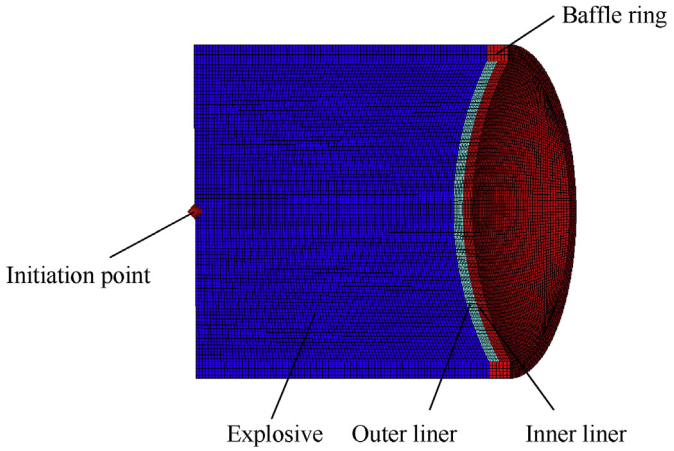

Fig. 4. Numerical model of warhead with double-layer liners.

Table 2
Parameters of copper and 45# steel.

material	ρ/(g·cm^{-3})	A'/GPa	B'/GPa	C	n	m
copper	8.96	0.090	0.292	0.025	0.31	1.09
45#steel	7.83	0.792	0.510	0.014	0.26	1.03

steel liner forms a short and wide penetrator following.

Concerning the type D liners, it reveals that the outer copper liner forms an EFP with a certain length-diameter ratio. However, the aluminum liner fragments, melts and vapors.

The morphologies of tandem EFPs revealed in the X-ray photographs, which are taken at two different instances in four experiments, are essentially identical to those obtained from the numerical simulations, thus confirming the validity of the numerical simulations. The experimental and numerical data are presented in Table 5. By comparing these results, it is found that the deviations between the experimental and numerical values of the EFPs are in an acceptable range, indicating the numerical results are in good agreement with the experimental data.

3. Formation mechanism

In contrast to single-layer liner, there is a free interface between the double-layer liners, and the two liners can impact or slide with each other owing to the shock and acceleration caused by the detonation wave and the corresponding gaseous products. To investigate the separation of the inner and outer liners during the formation of tandem EFPs, the double-layer liners with the same thickness of 1.5 mm and the same copper material are designed.

Table 3
Parameters of aluminum.

ρ/(g·cm^{-3})	A'/GPa	B'/GPa	a	b	α	β	e_0/(kJ·g^{-1})	e_s/(kJ·g^{-1})	e_{sd}/(kJ·g^{-1})
2.79	0.749	0.65	0.5	1.63	5	5	5	3	15

Table 4
Comparison between experiments and simulations.

No.	Type	$t_1 = 150$ μs	$t_2 = 210$ μs
1	A	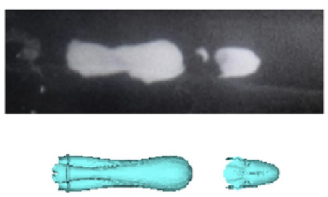	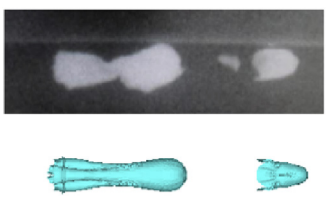
2	B	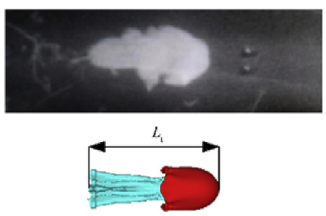	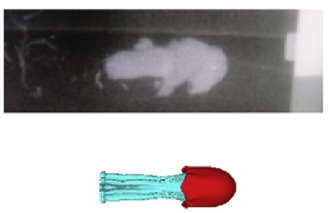
3	C	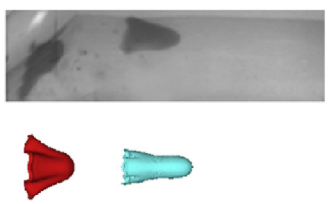	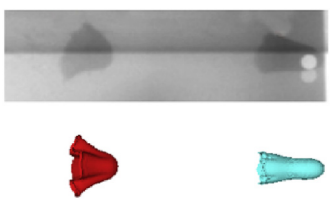
4	D	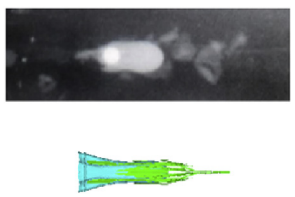	–

Please cite this article as: Ma H-b et al., Formation and impact-induced separation of tandem EFPs, Defence Technology, https://doi.org/10.1016/j.dt.2019.09.003

Table 5
Experimental and simulated data.

No.	Parameters	$t_1 = 150$ μs		Error/(%)	$t_2 = 210$ μs		Error/(%)
		Experiment	Simulation		Experiment	Simulation	
1	$V_o\|V_i$	1410|1641	1437|1796	1.91|9.45	1401|1639	1435|1793	2.43|9.40
	$L_o\|L_i$	43.08|15.38	45.09|16.96	4.67|10.27	47.08|16.00	48.31|17.40	2.61|8.75
	$D_o\|D_i$	15.38|10.15	14.50|9.20	−5.72|-9.36	15.23|10.15	14.50|9.10	−4.79|-10.34
2	$V_o\|V_i$	1608|1626	1491|1667	−7.28|2.52	1601|1620	1487|1663	−7.12|2.65
	L_t	47.49	50.84	7.05	53.81	57.21	6.32
	$D_o\|D_i$	-|17.54	14.12|18.61	-|6.10	-|17.54	13.22|18.61	-|6.10
3	$V_o\|V_i$	1350|1731	1394|1780	3.26|2.83	1344|1723	1367|1775	1.71|3.02
	$L_o\|L_i$	23.54|33.23	24.88|35.49	5.69|6.80	23.82|33.96	24.92|36.31	4.62|6.92
	$D_o\|D_i$	16.12|11.88	16.82|12.41	4.34|4.46	15.94|11.65	16.82|12.41	5.52|6.52
4	$V_o\|V_i$	–	–	–	–	–	–
	$L_o\|L_i$	45.10|-	45.77|-	1.49|-	–	–	–
	$D_o\|D_i$	14.30|-	12.76|	−10.77|-	–	–	–

Note: the parameters of *V*, *L*, *D* are EFP velocity, length and head diameter, respectively; the subscripts i, o and t denotes inner liner (foregoing EFP), outer liner (following EFP) and united EFP, respectively; the units of *V*, *L*, *D* are m/s, mm and mm, respectively.

The formation of tandem EFPs is then analyzed by studying the velocity variations of two EFPs. Actually, the formation process of tandem EFPs may be divided to four phases: impact phase, propulsion phase, slide phase and free flight phase. The impact phase is illustrated in Fig. 5. Considering the impact on the axis as an example, the center of the outer liner is firstly accelerated by the shock wave, which is then transmitted to the inner liner and reflected at the free interface to form a tensile wave. Owing to the combined actions of the transmitted shock wave and reflected tensile wave, the inner liner gains an axial velocity that is greater than that of the outer liner, thus producing a gap between the inner and outer liners at the axis. The outer liner continues to accelerate owing to the actions of the detonation products and quickly catches up to the inner liner. This causes a second impact and thus, a second separation. Due to the detonation products, the outer and inner liners repeat the "catch up-impact-separation-catch up" process, until the detonation products no longer have a significant effect on the outer liner.

The axial velocity curves on the axis of tandem FEPs with a comparison of a single EFP are shown in Fig. 6. It is noted that the total mass of double liners is the same as that of a single liner. It can be seen that the velocity of the single EFP increases consecutively before the time of 27.7 μs, and then drops gradually. However, the velocities of tandem EFPs are more complex. In fact, the velocities of the double-layer liners rise in turns between 6.0 μs and 14.0 μs,

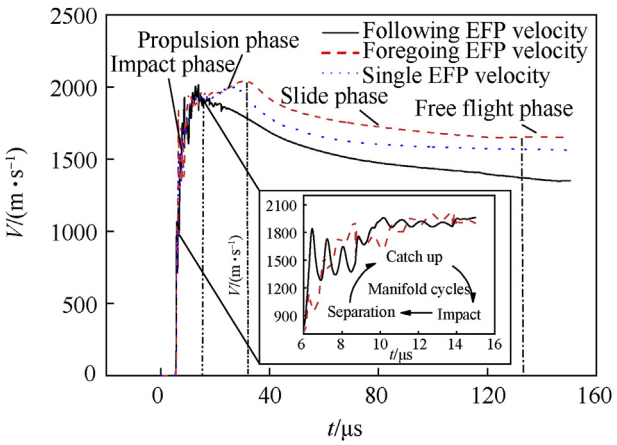

Fig. 6. The axial velocity curves on the axis of tandem FEPs with a comparison of a single EFP.

owing to impact between the two liners. These changes in velocity are also accompanied by an exchange of kinetic energy between the two liners. After multiple impacts, the foregoing EFP would have a higher velocity than that of the following EFP. Therefore, during the formation of tandem EFPs, multiple impacts will occur between the

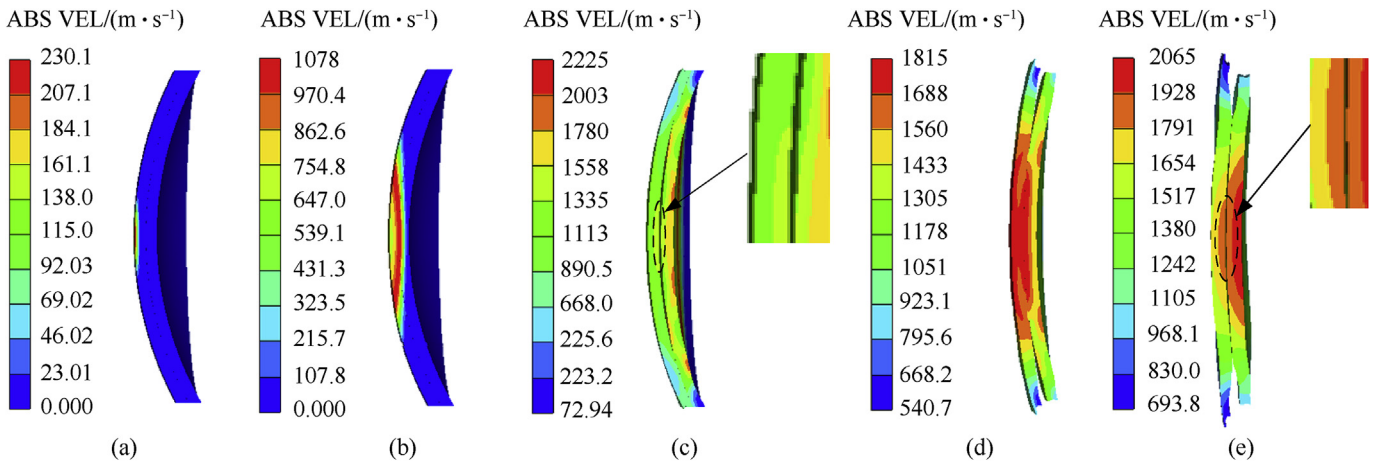

Fig. 5. Impact phase: (a) the shock wave propagating to the outer liner at the time of 5.4 μs; (b) the shock wave transmitting to the inner liner at the time of 5.8 μs; (c) the impact and reflected wave-induced gap between two liners at the time of 7.0 μs; (d) the outer liner is accelerated by the detonation products and the second impact occurs at the time of 9.0 μs; (e) the gap appears again at the time of 10.7 μs.

Please cite this article as: Ma H-b et al., Formation and impact-induced separation of tandem EFPs, Defence Technology, https://doi.org/10.1016/j.dt.2019.09.003

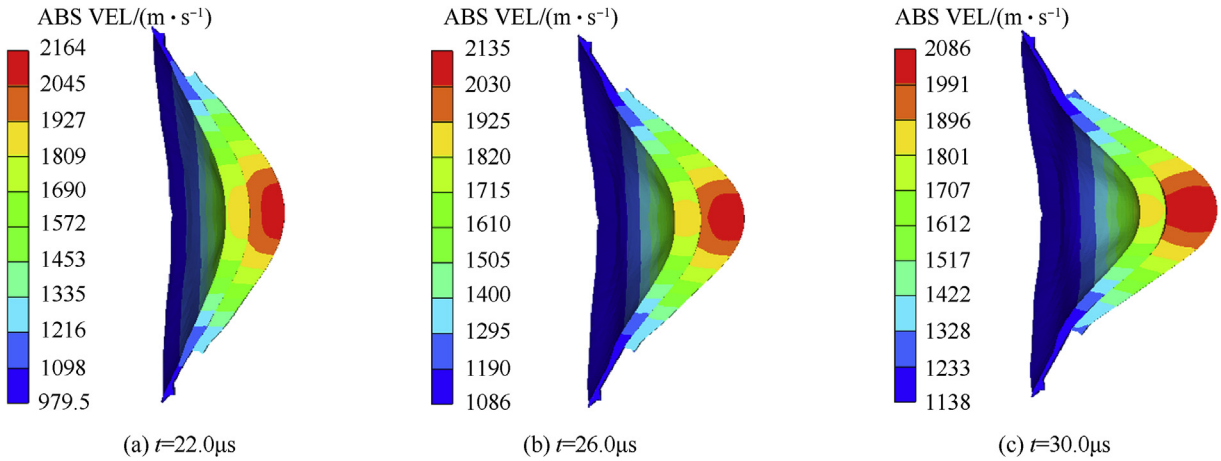

Fig. 7. Propulsion phase: (a) $t = 22.0$ μs; (b) $t = 26.0$ μs; (c) $t = 30.0$ μs.

inner and outer liners at different positions. Kinetic energy would be exchanged during this process, ultimately resulting in significantly different axial velocities for the outer and inner liners.

Then, the formation of the tandem EFPs enters the propulsion phase, which is illustrated in Fig. 7. Combined with Fig. 6, it can be found that the foregoing EFP accelerates consecutively, but the following EFP slows correspondingly in the propulsion phase. This phenomenon indicates the impact in this stage is insignificant, while the outer liner is likely to push the inner liner forward for about 16.3 μs. At the same time, outer and inner liners both flip and close to form EFPs gradually.

Subsequently, the slide phase is to begin and the process is shown in Fig. 8. The foregoing and following EFPs slide relatively and separate gradually, owing to differences in their velocities. In this phase, impacts between the outer and inner liners mainly occur in the radial direction instead of the axial direction. Based on Fig. 6, it can be concluded that the radial impacts have a negligible effect on the axial velocities of the two EFPs. Nonetheless, it is observed that the closing velocity at the rear of the inner liner is greater than that at the front of the outer liner. As such, the rear of the inner liner closes to the front of the outer liner, which finally results in a certain degree of deformation, or even necking for the two EFPs.

Finally, the two EFPs no longer contact with each other at 150 μs approximately, and the morphologies and velocities of the two EFPs become stable. Thus, the two EFPs switch to the free flight stage, as

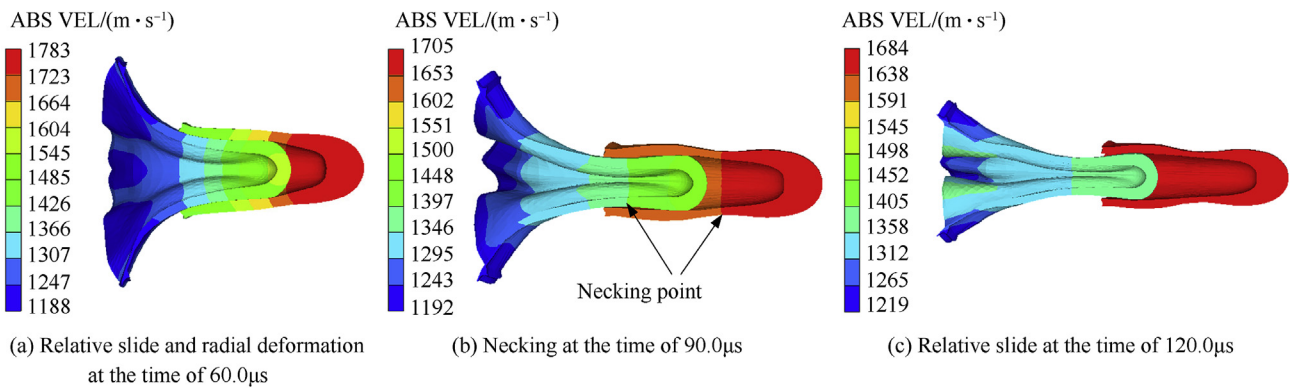

Fig. 8. Slide phase: (a) relative slide and radial deformation at the time of 60.0 μs; (b) necking at the time of 90.0 μs; (c) relative slide at the time of 120.0 μs.

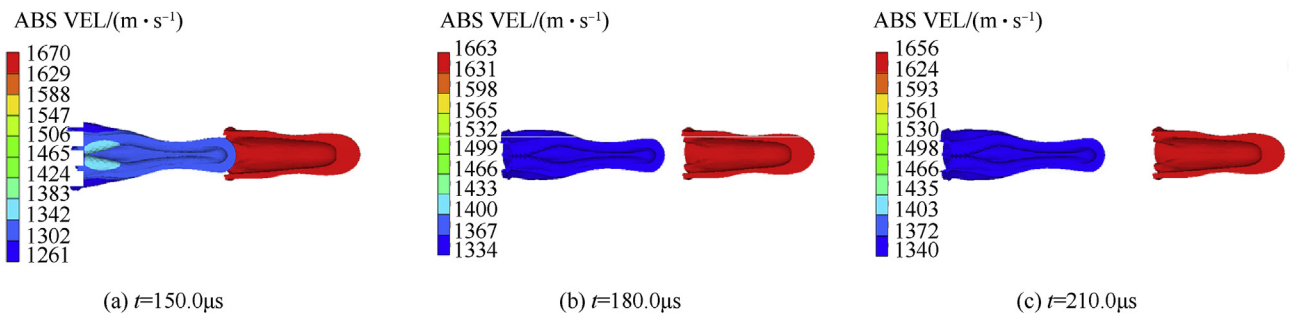

Fig. 9. Free flight phase: (a) $t = 150.0$ μs; (b) $t = 180.0$ μs; (c) $t = 210.0$ μs.

Please cite this article as: Ma H-b et al., Formation and impact-induced separation of tandem EFPs, Defence Technology, https://doi.org/10.1016/j.dt.2019.09.003

shown in Fig. 9.

4. Influence mechanism

The formation mechanism of tandem EFPs has been discussed above. However, further work should be conducted to study the influence mechanism on the formation behavior.

4.1. Influences of material match

The material match of the outer and inner liners influences the formation process greatly. Fig. 10 shows the velocity curves of tandem EFPs with different types. It should be noted that all the outer and inner liners have a thickness of 1.5 mm in this section. Combined with Fig. 6, the results show both the type A liners and the type C liners have a large velocity difference between the foregoing and following EFPs. While the type B liners form two EFPs with a relatively small velocity difference. Moreover, the type D liners have the maximum velocities for both the foregoing and following EFPs. However, the foregoing aluminum EFP velocity terminates at the time of 23.9 μs. These significant different phenomena are highly relative to the formation process.

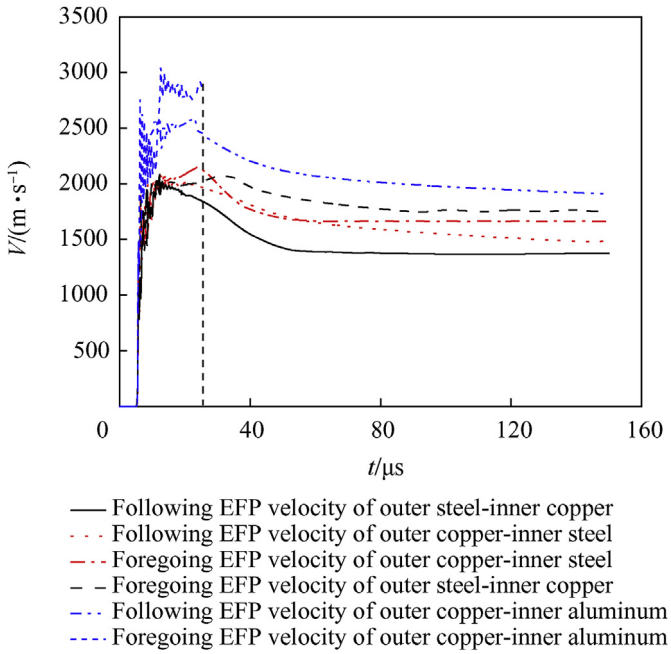

Fig. 10. Comparison of the velocity curves of different tandem EFPs among types B, C and D.

As for the type B, the formation process is shown in Fig. 11. The steel liner forms an EFP with a small length-diameter ratio because of the high strength of steel, while the outer copper liner remains to form a long EFP due to the low strength and ideal ductility of copper. It is noted that the velocity difference in this case is significantly less than that in the situation of type A. For mechanism considerations, on one hand, the kinetic energy interaction process for type B liners is similar to a special case that a "soft" metal impacting and pushing forward a "hard" metal. As such, more kinetic energy is translated to deformation energy for the "soft" metal, which may decrease the velocity to some extent; on the other hand, the steel EFP from the high strength liner would have a larger cavity diameter, resulting in a radial gap between the two liners. Thus, the following copper EFP cannot accelerate the foregoing steel EFP very well. Actually, the push duration is only about 13.5 μs in this case. In addition, the foregoing steel EFP has a small density and a large diameter, and its velocity attenuation is significantly faster than that of the following copper EFP during flight. As such, compared with the type A tandem EFPs, the type B tandem EFPs need a longer time of about 200 μs for separation.

Contrarily, the formation of type C tandem EFPs is depicted in Fig. 12. It can be seen that the inner copper liner forms a long EFP, while the outer steel liner remains to become a short EFP due to the high strength. The velocity difference in this case is the most significant. For mechanism considerations, for one thing, the kinetic energy interaction process for type C liners is much like the case that a "hard" metal impacting and pushing forward a "soft" metal. As such, more kinetic energy is transmitted to the foregoing "soft" metal for its formation and acceleration; for another, the radial closing velocity of copper liner is higher than that of steel liner, causing a tight contact between the foregoing EFP rear and the following EFP head, which is beneficial for the following EFP to push the foregoing one. The push duration is about 19.7 μs in this case. Furthermore, the velocity of following steel EFP decays more quickly, improving the velocity difference of two EFPs and leading to less separation time of about 90 μs. In addition, the tight contact also results in the head of following EFP being pressed and the closing of the rear of foregoing EFP being prevented to some extent. Finally, a cone steel EFP and a long copper EFP with a larger rear diameter are obtained, respectively.

The formation process of type D tandem EFPs is displayed in Fig. 13. It is found that only a copper EFP with some aluminum debris are obtained in this case. For mechanism considerations, the intensive impact during the kinetic energy interaction process may lead to the aluminum liner being melted, vapored and fractured, owing to low melting point, low boiling point and expansion

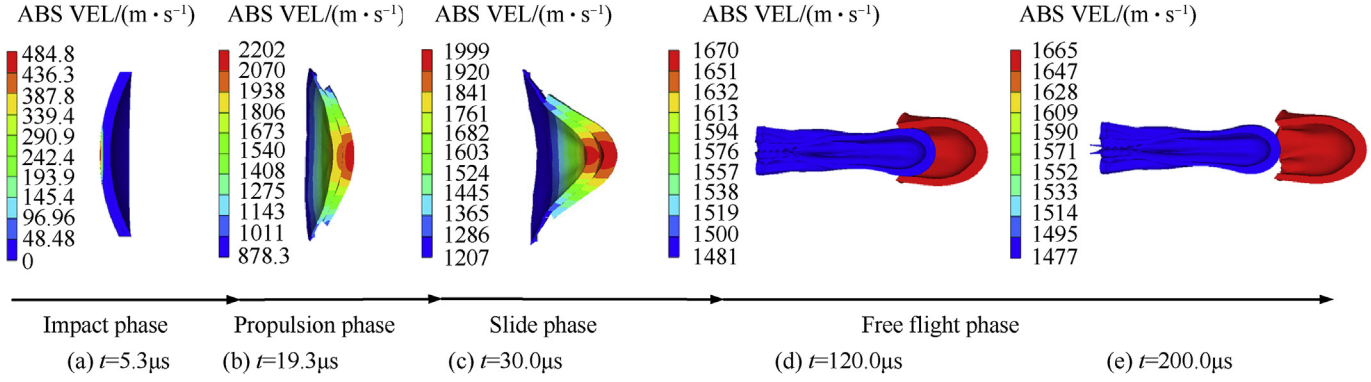

Fig. 11. Formation process of tandem EFPs from type B liners: (a) $t = 5.3$ μs; (b) $t = 19.3$ μs; (c) $t = 30.0$ μs; (d) $t = 120.0$ μs; (e) $t = 200.0$ μs.

Please cite this article as: Ma H-b et al., Formation and impact-induced separation of tandem EFPs, Defence Technology, https://doi.org/10.1016/j.dt.2019.09.003

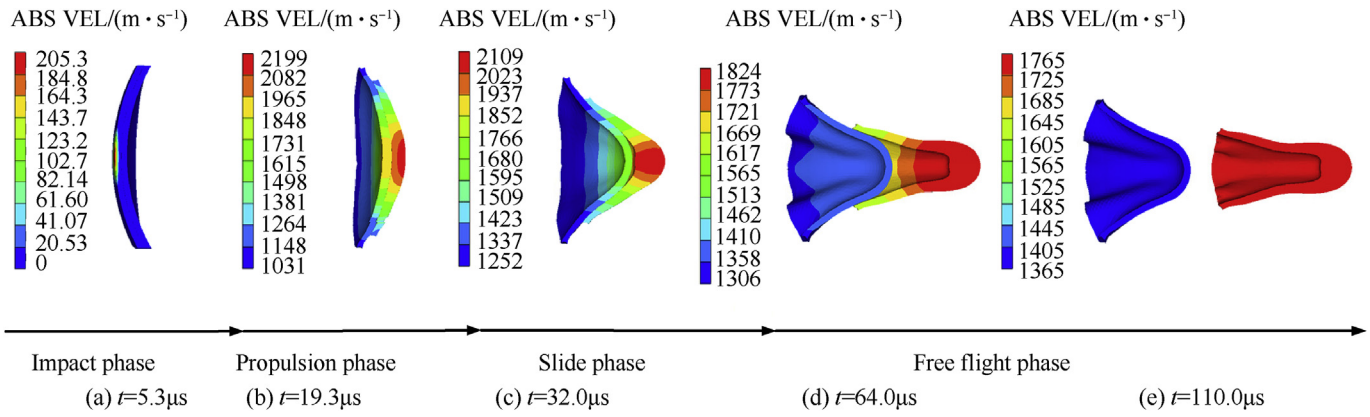

Fig. 12. Formation process of tandem EFPs from type C liners: (a) $t = 5.3$ μs; (b) $t = 19.3$ μs; (c) $t = 32.0$ μs; (d) $t = 64.0$ μs; (e) $t = 110.0$ μs.

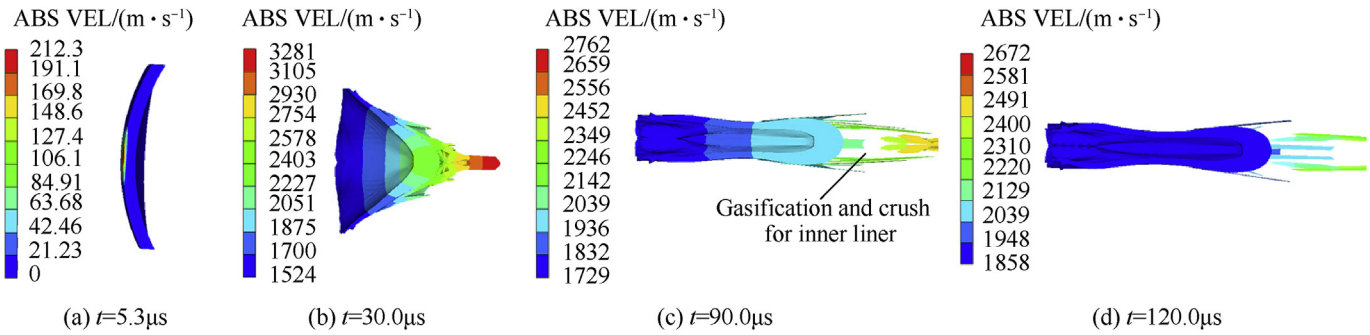

Fig. 13. Formation process of tandem EFPs from type D liners: (a) $t = 5.3$ μs; (b) $t = 30.0$ μs; (c) $t = 90.0$ μs; (d) $t = 120.0$ μs.

behavior of aluminum.

4.2. Influences of thickness match

Based on the above findings, it may be concluded that type D liners cannot form tandem EFPs. Therefore, the subsequent numerical simulations mainly focus on the form processes of tandem EFPs from other types of double liners. The total thickness of the double liners is kept constant at 3 mm, and the primary objective of these simulations is to examine the effects of the liner thickness ratio on the forming processes. The thickness ratio between the outer and inner liners (H_o/H_i) is set to 1/2, 5/7, 1, 7/5, and 2 in the numerical simulations.

Table 6~8 discuss the influences of H_o/H_i on the morphology, length, and length-diameter ratio of tandem EFPs. The results show the interaction between two EFPs becomes insignificant after the time of 150 μs. Therefore, a comparative analysis is conducted based on the characteristics of tandem EFPs at 150 μs.

As for the type A liners, it is evident that the decreases in H_o/H_i lead to increases in the length and length-diameter ratio for both foregoing and following EFPs in Table 6. For the mechanism considerations, decreases in the thickness of the outer liner should cause corresponding increases in the thickness of the inner liner, thus increasing the mechanical strength of the inner liner. Therefore, the inner liner becomes harder to deform, which increases the time required to separate the inner and outer liners, and thus the longer time for the detonation products to act on the double liners. This is beneficial for the formation behavior, which results in higher

Table 6
The influences of thickness match on type A EFPs.

H_o/H_i	1/2	5/7	1	7/5	2
Outer copper | Inner copper	Penetrator	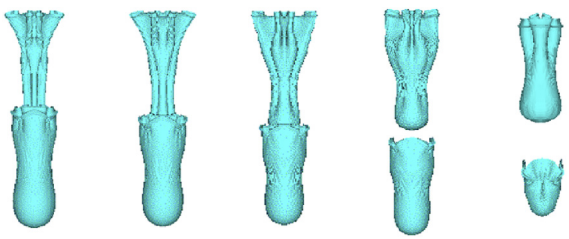			
	$L_o\|L_i$	54.15|48.24	50.61|44.31	48.62|40.1	47.23|38	45.09|16.96
	$L_o/R_o\|L_i/R_i$	6.37|3.65	5.41|3.46	4.88|3.22	4.48|3.19	3.11|1.84

Note: the parameter of R is EFP head diameter.

Please cite this article as: Ma H-b et al., Formation and impact-induced separation of tandem EFPs, Defence Technology, https://doi.org/10.1016/j.dt.2019.09.003

length-diameter ratios and therefore, more ideal tandem EFPs. Conversely, if the thickness of the outer liner is increased, the thin inner liner will separate from the outer liner more quickly. Although the thin inner liner is easier to deform, the time for the detonation products to act on the inner liner is now much shorter owing to the excessively fast separation of the inner and outer liners, which results in insufficient liner deformation. This leads to the formation of a penetrator with a relatively low length-diameter ratio for the inner liner. Furthermore, the outer liner is harder to deform owing to its increased thickness, finally the outer liner also shape an EFP with low length-diameter ratio.

According to Table 7, variations in the liner thickness do not greatly influence the EFP morphology when steel is used as the inner liner material. This is because the mechanical strength of steel is significantly greater than that of copper. In these numerical simulations, it is found that decreases in H_o/H_i are without significantly altering for the length of the foregoing EFP, but it slightly reduces the length-diameter ratio. Moreover, the length and length-diameter ratio of the following EFP also change slightly with decreases in H_o/H_i.

With regard to type C liners showed in Table 8, it is found that with decrease of H_o/H_i, the length and length-diameter ratio for both the foregoing and following EFPs increase. These regulars of type C liners are qualitatively similar to those of type A liners observed in Table 6.

Based on Fig. 14, it is found that liners of different types have the same regular pattern in velocity differences. With the H_o/H_i decreasing, the velocity differences drop gradually.

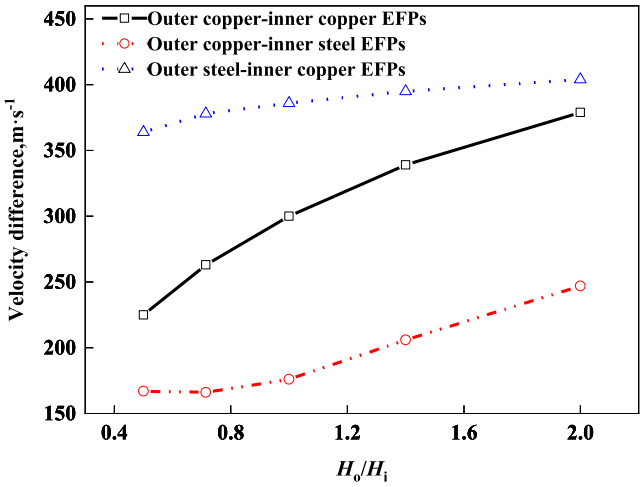

Fig. 14. Comparison of the influences of thickness match on velocity differences among types of A, B and C.

5. Conclusions

(a) The formation behavior of tandem EFPs includes four phases, such as impact phase, propulsion phase, slide phase and free flight phase. During the impact phase, the velocities of the double-layer liners rise in turns, owing to the repeat of "catch up-impact-separation-catch up" process between the two

Table 7
The influences of thickness match on type B EFPs.

H_o/H_i		1/2	5/7	1	7/5	2
Outer copper | Inner steel	Penetrator	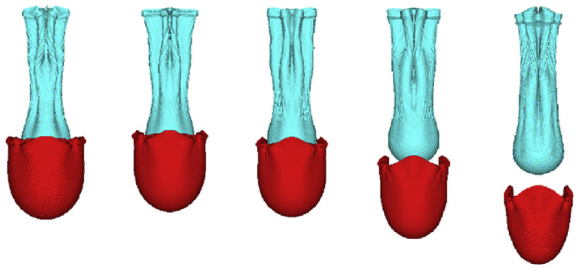				
	$L_o\|L_i$	49.97|25.02	47.2|25.1	48.82|24.86	48.08|25.45	50.28|24.55
	$L_o/R_o\|\ L_i/R_i$	3.75|1.25	3.59|1.29	3.68|1.33	3.55|1.43	3.62|1.46

Note: the parameter of R is EFP head diameter.

Table 8
The influences of thickness match on type C EFPs.

H_o/H_i		1/2	5/7	1	7/5	2
Outer steel | Inner copper	Penetrator	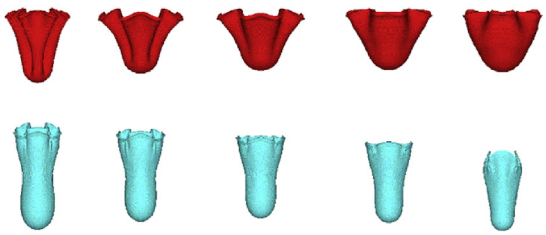				
	$L_o\|L_i$	28.98|41.41	25.88|36.88	24.88|35.49	24.56|32.25	24.53|31.58
	$L_o/R_o\|L_i/R_i$	2.60|3.12	1.74|2.96	1.48|2.86	1.40|2.83	1.29|2.78

Note: the parameter of R is EFP head diameter.

Please cite this article as: Ma H-b et al., Formation and impact-induced separation of tandem EFPs, Defence Technology, https://doi.org/10.1016/j.dt.2019.09.003

liners. In the propulsion phase, the impact is insignificant, and the outer liner would push the inner liner forward. It is noted that there is significant kinetic energy exchange during the impact and propulsion phases, causing the two EFPs separating gradually. Then, the radial impacts in the slide phase have a negligible effect on the axial velocities of the two EFPs. However, the radial interaction between two liners produces important influences on the appearance of tandem EFPs, and even results in necking phenomenon. At last, the two EFPs no longer contact with each other and begin to flight freely.

(b) The formation behavior significantly depends upon the material match of the two liners. If the outer and inner liners have the same thickness, the outer copper-inner copper liners are most likely to form two long EFPs with a medium separation time. The outer copper-inner steel liners form a foregoing short steel EFP and a following long copper EFP, with a longest separation time. The outer steel-inner copper liners become a foregoing long copper EFP and a following conical steel EFP, with a least separation time. It should be mentioned that the outer copper-inner aluminum liners fail to form the tandem EFPs, due to low melting point, low boiling point and expansion behavior of aluminum.

(c) The formation behavior also lies on the thickness match of the two liners. For both outer copper-inner copper liners and outer steel-inner copper liners, the length and length-diameter ratio of both foregoing and following EFPs increase gradually, with the thickness ratio of outer liner to inner liner decreasing. However, in concern of outer copper-inner steel liners, the high strength of steel causes the thickness variation is no longer the key parameter for the formation behavior.

(d) The interaction of tandem EFPs is complex, and more work should be carried out in the future, such as: more kinds of material match need to be studied, the flight stability of tandem EFPs should be stressed, and the penetration mechanism also needs to be researched.

References

[1] Tosello R, Vives M, Tronche A. Twin EFPs for underwater applications. In: Proceedings of the 16th international symposium on ballistics. San Francisco, USA: I B C; 1996. p. 357–68.

[2] Weimann K, Blache A. An explosively formed projectile with tantalum penetration and steel stabilization base. In: Proceedings of the18th international symposium on ballistics. San Antonio, TX, US: I B C; 1999. p. 22–5.

[3] Fong R, Weimann K. Testing and analysis of multi-liner EFP warhead. In: Proceedings of the 20th international symposium on ballistics. Orlando, FL, US: I B C; 2002. p. 578–82.

[4] Zheng Yu, Wang Xiaoming, Li Wenbin, et al. Formation of shaped charge with double layer liners into tandem EFP. Explos Shock Waves 2012;32(1):29–33.

[5] Li Huiming, Zhang Huaizhi, Zhao Donghua, et al. The study on the effect of inner and outer layer of material properties of double-layer EFP. J Proj Rocket Missiles Guid 2012;32(6):81–2.

[6] Yuan Long, Mao Zhengxing, Liu Jianfeng, et al. Influence of curvature radius on The formation and penetration of explosively formed penetrator warhead of the double layer liner. Explos Mater 2016;45(3):5–10.

[7] Yuan Long, Liu Jianfeng, Chong Ji, et al. Numerical simulation on formation and penetration of double-layer liners EFP warhead influenced by multi-point initiation. Acta Armament 2016;(12).

[8] Wang Zhe, Jiang Jianwei, Wang Shuyou, et al. A calculation model of velocity of tandem EFP with double layer liners. Acta Armamentarii 2017;(07):56–61.

[9] He Jing, Wang Zhijun, Sun Hua, et al. Numerical simulation and analysis on formation of series EFP with double liners. Ordnance Mater Sci Eng 2013;36(5):103–5.

[10] Guo Huanguo, Zheng Yuanfeng, Yu Qingbo, et al. Penetration behavior of reactive liner shaped charge jet impacting thick steel plates. Int J Impact Eng 2019;126:76–84.

[11] Teng Taoju, Lei Chen, Shi Xiang. Numerical simulation on formation process and penetration performance of double layer liners EFP with different materials. J Proj Rocket Missiles Guid 2014;34(5):264–75. 2017, 109.

[12] Liu Jianfeng ,Long Yuan, Ji Chong, et al. The influence of liner material on the dynamic response of the finite steel target subjected to high velocity impact by explosively formed projectile. Int J Impact Eng,264-275.

[13] Wang Haifu, Feng Shunshan, Liu Youying. Introduction to space debris. Science Press; 2010. p. 211–3.

Please cite this article as: Ma H-b et al., Formation and impact-induced separation of tandem EFPs, Defence Technology, https://doi.org/10.1016/j.dt.2019.09.003